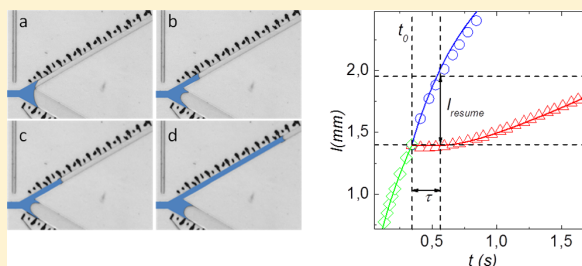


# Meniscus Arrest during Capillary Rise in Asymmetric Microfluidic Pore Junctions

Zeinab Sadjadi,<sup>\*,†</sup> Michael Jung,<sup>‡,§</sup> Ralf Seemann,<sup>‡,§</sup> and Heiko Rieger<sup>†</sup><sup>†</sup>Theoretical Physics and <sup>‡</sup>Experimental Physics, Saarland University, 66041 Saarbrücken, Germany<sup>§</sup>Max Planck Institute for Dynamics and Self Organization, 37077 Göttingen, Germany

**ABSTRACT:** The capillary rise of liquid in asymmetric channel junctions with branches of different radii can lead to long-lasting meniscus arrests in the wider channel, which has important implications for the morphology and dynamical broadening of imbibition fronts in porous materials with elongated pores. Using a microfluidic setup, we experimentally demonstrate the existence of arrest events in Y-shaped junctions, and measure their duration and compare them with theoretical predictions. For various ratios of the channel width and liquid viscosities and for different values of the feeding channel length, we find that the meniscus within the wider branch is arrested for a time that is proportional to the time that the meniscus needed to reach the junction, in very good quantitative agreement with theoretical predictions.



## 1. INTRODUCTION

Fluid flow through porous media has been a topic of considerable interest due to its scientific importance and practical applications.<sup>1–3</sup> Among others, imbibition in disordered media plays a fundamental role in various industrial areas, ranging from paper and textile treatment to oil recovery and groundwater hydrology.<sup>1,4</sup> Spontaneous imbibition is a particular type of fluid advancement into a medium driven by capillary force. The average position of the liquid front follows the Lucas–Washburn scaling law,<sup>1,5,6</sup> which turned out to remain valid down to nanoscopic pore scales<sup>7–9</sup> independent of the geometrical complexity of the porous medium.

In most porous materials such as paper and sand, the propagating imbibition front forms a single connected interface between the propagating and the displaced liquid,<sup>10</sup> giving rise to dynamical roughening behavior described by universal scaling laws.<sup>11–15</sup> For pore networks, in which the porous space forms a three-dimensional random network of interconnected pipes with a sufficiently large aspect ratio (ratio between pipe length and radius), the interface between the propagating and the displaced liquid is disconnected and consists of many isolated menisci.<sup>2,16,17</sup> The characteristics of the imbibition dynamics of this ensemble of menisci in such pore networks can be expected to be very different from the propagation of continuous interfaces in random media. In Figure 1, a schematic sketch of imbibition in porous material with short and elongated pores is illustrated. Indeed, a recent experiment on nanoporous Vycor glass (NVG) representing a pore network of elongated pores with an aspect ratio of between 5 and 10 showed anomalously fast imbibition front roughening.<sup>18</sup> The width of the imbibition front, which is the

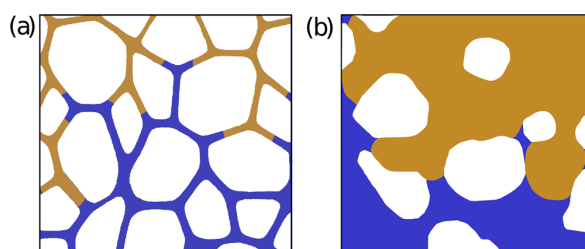


**Figure 1.** Schematic shape of the imbibition front in porous structure consisting of (a) large and (b) short aspect ratio pores.

distance between the most- and the least-advanced menisci, grows rapidly with time with a growth exponent of close to  $1/2$ .

Recently a scaling theory for spontaneous imbibition in pore networks with elongated pores was proposed,<sup>19</sup> which relies on the hypothesis of meniscus arrest at asymmetric pore junctions, i.e., junctions with pores of different radii. The arrest times were predicted to be proportional to the time that the front needs to reach the adjacent junctions, which implies that the front width scales in the same way with time as the average front position, i.e., with an exponent of  $1/2$ . This theory could explain the dynamics of spontaneous imbibition in pore networks with elongated pores. One expects that meniscus arrest at channel junctions in pore networks is cooperative, which means that the time at which a channel is filled depends on the fluid configuration in adjacent channels beyond the nearest

**Received:** October 20, 2014

**Revised:** January 23, 2015

**Published:** February 9, 2015

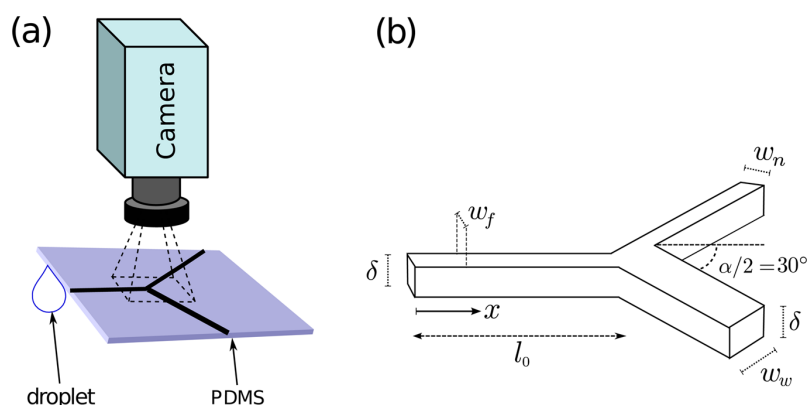


Figure 2. (a) Schematic of the experimental setup. (b) Detailed structure of a Y junction.

Table 1. Different Types of Y-Junction Geometries Labeled A–H, with the Variation in the Length of the Feeding Channel Indicated with a Number

geometry	$W_f$ [ $\mu\text{m}$ ]	$W_n$ [ $\mu\text{m}$ ]	$W_w$ [ $\mu\text{m}$ ]	$l_0$ [ $\mu\text{m}$ ]	$W_w/W_n$	$\tau$ [s]	$l_{\text{resume}}$ [mm]
A1	$52 \pm 1$	$47 \pm 1$	$83 \pm 1$	$1070 \pm 150$	1.8	$0.08 \pm 0.02$	$0.14 \pm 0.02$
A2	$53 \pm 1$	$44 \pm 1$	$82 \pm 1$	$3300 \pm 80$	1.8	$1.48 \pm 0.04$	$0.58 \pm 0.02$
A3	$53 \pm 1$	$44 \pm 1$	$82 \pm 1$	$3700 \pm 40$	1.8	$0.66 \pm 0.04$	$0.79 \pm 0.02$
A4	$50 \pm 1$	$40 \pm 1$	$85 \pm 1$	$5100 \pm 150$	2.1	$0.46 \pm 0.04$	$1.22 \pm 0.02$
B1	$53 \pm 3$	$44 \pm 2$	$122 \pm 3$	$1400 \pm 80$	2.9	$0.22 \pm 0.02$	$0.44 \pm 0.02$
B2	$59 \pm 1$	$45 \pm 1$	$131 \pm 1$	$3600 \pm 230$	2.9	$0.92 \pm 0.04$	$1.12 \pm 0.02$
B3	$59 \pm 1$	$45 \pm 1$	$131 \pm 1$	$5500 \pm 150$	2.9	$3.42 \pm 0.04$	$2.06 \pm 0.02$
B4	$59 \pm 1$	$45 \pm 1$	$131 \pm 1$	$8800 \pm 120$	2.9	$7.14 \pm 0.04$	$2.95 \pm 0.02$
C1	$49 \pm 1$	$37 \pm 1$	$50 \pm 1$	$960 \pm 140$	1.4	$0.01 \pm 0.02$	$0.03 \pm 0.02$
C2	$48 \pm 2$	$37 \pm 1$	$54 \pm 1$	$1270 \pm 140$	1.5	$0.03 \pm 0.02$	$0.06 \pm 0.02$
D1	$57 \pm 1$	$44 \pm 2$	$70 \pm 1$	$1020 \pm 70$	1.6	$0.03 \pm 0.02$	$0.09 \pm 0.02$
D2	$55 \pm 3$	$45 \pm 1$	$68 \pm 2$	$1340 \pm 130$	1.5	$0.03 \pm 0.02$	$0.08 \pm 0.02$
D3	$56 \pm 1$	$45 \pm 1$	$68 \pm 1$	$1540 \pm 130$	1.5	$0.06 \pm 0.02$	$0.11 \pm 0.02$
E	$50 \pm 1$	$38 \pm 1$	$66 \pm 1$	$990 \pm 180$	1.7	$0.06 \pm 0.02$	$0.15 \pm 0.02$
F1	$52 \pm 1$	$44 \pm 2$	$102 \pm 1$	$1020 \pm 100$	2.3	$0.11 \pm 0.02$	$0.31 \pm 0.02$
F2	$50 \pm 1$	$41 \pm 1$	$99 \pm 1$	$1180 \pm 180$	2.4	$0.17 \pm 0.02$	$0.41 \pm 0.02$
G1	$59 \pm 1$	$49 \pm 1$	$169 \pm 2$	$790 \pm 60$	3.4	$0.08 \pm 0.02$	$0.29 \pm 0.02$
G2	$60 \pm 3$	$50 \pm 2$	$172 \pm 3$	$1520 \pm 90$	3.4	$0.31 \pm 0.02$	$0.73 \pm 0.02$
H	$51 \pm 1$	$39 \pm 2$	$137 \pm 1$	$1190 \pm 130$	3.5	$0.22 \pm 0.02$	$0.50 \pm 0.02$

neighbors.<sup>20</sup> Computer simulations of a pore network model show clear indications of this cooperativity.<sup>19</sup>

In this article we study the capillary rise of liquid in asymmetric Y-shape pore junctions experimentally using a microfluidic setup and compare it with the theoretical predictions. Particular focus will be on the meniscus arrest and its dependence on geometrical parameters, namely, the lifetimes of, according to ref 21, very stable meniscus configurations inside pore junctions. A related channel geometry can be found in the pore-doublet model,<sup>22,23</sup> which consists of two parallel channels of different radii attached to a common feeding and exit channel via Y junctions. Until now only the different meniscus travel times in the two channels have been studied<sup>22,23</sup> but not the arrest time of the meniscus of the wider channel at the feeding junction, which we do in this article. In a network composed of Y junctions, some nonwetting phases become trapped, which broadens the front.<sup>18</sup> A similar sketch is demonstrated in Figure 4 of ref 18.

The article is organized as follows. Section 2 is devoted to the description of the microfluidic experimental setup. The details of the theoretical modeling of spontaneous imbibition in Y-shaped channels are presented in section 3. In section 4 the

experimental results are presented and discussed by comparing them with the theoretical predictions. Finally, the article is concluded in section 5.

## 2. EXPERIMENTAL SECTION

A Y-shaped junction is considered in a planar microfluidic device (Figure 2), which allows us to neglect the hydrostatic pressure. The junction consists of three rectangular channels: a feeding channel of width  $w_f$  and length  $l_0$  where the liquid enters the device and two branch channels, one of them having a wider channel width  $w_w$  and another one having a narrow with width  $w_n$  ( $w_n < w_w$ ). In all experiments  $w_n < w_f < w_w$ , although  $w_f$  is not restricted in the theoretical approach.

The two branch channels are symmetric with respect to the  $x$  axis whereas the opening angle of the Y junction is  $\alpha = 60^\circ$ . The microfluidic devices are fabricated from Sylgard 184 (Dow Corning) molded from photolithographically generated SU-8 (MicroChem Corp.) structures on silicon wafers.<sup>24</sup> The height of the positive SU-8 structures thus defines the channel height of the Sylgard device,  $\delta = 95 \pm 10 \mu\text{m}$ . After curing the Sylgard at  $70^\circ\text{C}$  for 5 h, we remove the PDMS rubber from the SU-8 master. Occasionally, dust particles which were previously on the master or small fragments from acute edges of the SU-8 master are included in the liquid Sylgard and remain

in the cured Sylgard after removal from the mold. Care was taken that these objects did not alter the advancing meniscus of an invading liquid. The Sylgard device and a cleaned glass microscopy slide are activated in nitrogen plasma (Diener Electronics) and bonded to each other. Subsequently, the closed device is heated for 2 h at 150 °C and given time to rest for another 12 h to guarantee a good bond and to restore the hydrophobic properties of the Sylgard and a reproducible wettability for the used liquid. The Sylgard devices are cut open at the channel ends, resulting in feeding channel lengths  $l_0$  ranging from 0.8 to 8.8 mm. The width of the feeding channel  $w_f$  ranges from 49 to 59  $\mu\text{m}$ , and the width of the wide channel  $w_w$  is varied between 52 and 171  $\mu\text{m}$  to achieve a ratio of  $w_w/w_n$  of between 1.4 and 3.5. Table 1 summarizes the geometrical parameters for all experimentally used devices.

Fluorinated oil FC-70<sup>25</sup> is used as a wetting liquid which does not swell the microfluidic device and thus guarantees constant channel geometry throughout the imbibition experiments. Each experiment was repeated three times and shows quantitatively reproducible results within the stated error bars. The error bars are determined by an accuracy of 10 images and depend on the time resolution used in the experiments. The fluorinated oil has a contact angle of  $\theta \approx 0^\circ$  with the device material as well as with the glass coverslip. The surface tension  $\sigma$  was determined to be  $\sigma_{\text{FC-70}} = 18 \pm 1$  mN/m using the pendant drop method.

By fitting the Lucas–Washburn law (section 3, eqs 2–4 and 6) to the liquid imbibing the straight feeding channel, we absorb several potential uncertainties into an effective viscosity  $\eta_{\text{eff}}$ . The most obvious ones are temperature variations in the laboratory, error in the channel geometry, local imperfections due to the roughness of the channel walls, and uncertainties in the experimentally determined surface tension. Of minor importance might be the uncertainty in the wettability of the Sylgard matrix by FC-70, a potential loss of FC-70 diffusing into the Sylgard matrix, and the shortcomings of the Lucas–Washburn law neglecting inertia effects. At a laboratory temperature of  $22 \pm 2$  °C, the viscosity is determined to be  $\eta_{\text{eff}} = 42 \pm 2$  mPa s. This value is a mean value averaged over several realizations at different laboratory temperatures using different devices. The statistical error mainly represents the influence of varying temperature. Potentially systematic errors resulting from other sources such as an error in the surface tension are not explicitly included. To compare experimental and theoretical imbibition behavior,  $\eta_{\text{eff}}$  is extracted from a particular experiment with an effective viscosity very close to the mean value (caption of Figure 7). The viscosity provided by the data sheet of the manufacturer<sup>25</sup> is about  $\eta = 27$  mPa s.

An experiment is started by placing a drop of approximate 5  $\mu\text{L}$  of the fluorinated oil on the cover slide right in front of the feeding channel, which spreads due to its small contact angle. After a short time, the spreading droplet reaches the microfluidic Y junction. An upper value of the positive Laplace pressure of a feeding droplet can be estimated to be  $P_L < 1$  Pa using a contact angle of  $<10^\circ$  for FC-70 on glass and an in-plane diameter of  $>2$  mm. Such a small Laplace pressure of the feeding droplet can be safely neglected with respect to the negative Laplace pressure of the meniscus in the microfluidic channels, which is about 1000 Pa. The liquid imbibition is observed through the glass slide of the device using an inverted microscope (Reichert-Jung MeF3) and a high-speed camera (Photron, SA3) with up to 500 fps at a resolution of  $1 \text{ k} \times 1 \text{ k}$  pixels. The sample was illuminated in transmission with an LED light source minimizing temperature and viscosity changes in the course of the experiment. The camera is continuously recording in continuous buffer mode, and recording is stopped when the liquid filaments are sufficiently long.

The recorded raw images are smoothed by applying an anisotropic filter using free available software ImageJ.<sup>26</sup> The subsequent analysis is conducted with Image Pro Plus 6.3 (Media Cybernetics). An image of the Y junction without liquid is subtracted from all other images in a time series. The resulting images showing just the liquid are segmented by applying a gray-level threshold to identify the menisci of the imbibing liquid. The positions  $l$  of the menisci in the narrow and wide channels are analyzed separately. The images are rotated so that the

respective channel is aligned horizontally and the horizontal coordinate of the center of the meniscus is determined automatically.

### 3. THEORETICAL PREDICTIONS

In the analytical treatment, the same type of Y junction is considered as described in the section 2. The dynamics of the liquid rise is governed by volume conservation, viscous drag, and capillary force, whereas gravity is negligible in the microfluidic device we intend to describe. In the theoretical considerations, we will neglect the volume of the Y junction that connects the three channels. The volume flux (liquid volume per time)  $Q$  of a laminar flow of a viscous fluid in a straight channel of length  $l$  is given by

$$Q = \frac{\Delta P}{l} c \quad (1)$$

where  $\Delta P$  is the pressure difference between the channel entry and the channel exit and  $c$  is a constant that depends on the viscosity,  $\eta$ , of the liquid and the geometry of the channel cross section. For cylindrical channels, it is  $c = \pi R^4/8\eta$  (with  $R$  being the radius of the circular cross section), and for rectangular channels, as considered in our experimental setup, it is<sup>27,28</sup>

$$c = \frac{\delta w^3}{\eta} f(\varepsilon) \quad (2)$$

where  $\varepsilon = w/\delta < 1$  and

$$f(\varepsilon) = \frac{1}{12} \left( 1 - \frac{192\varepsilon}{\pi^5} \sum_{i=0}^{\infty} \frac{\tanh\left[\frac{(2i+1)\pi}{2\varepsilon}\right]}{(2i+1)^5} \right) \quad (3)$$

The pressure difference at the liquid–gas interface, i.e., at the meniscus, in the channel is given by the Laplace pressure  $P_L = -2\sigma \cos \theta/R$  for a cylindrical channel with radius  $R$  and

$$P_L = -2\sigma \cos \theta \left( \frac{1}{w} + \frac{1}{\delta} \right) \quad (4)$$

for rectangular channels.

The capillary rise of the liquid within a channel is described by the time dependence of the distance  $l(t)$  of the meniscus from the channel entry, which is according to eq 1

$$Q = A \frac{dl}{dt} = \frac{P_{l=0} - P_L}{l} c \quad (5)$$

where  $A$  is the cross-sectional area of the channel, i.e.,  $A = \pi R^2$  for cylindrical channels and  $A = w\delta$  for rectangular channels, and  $P_{l=0}$  is the pressure at the channel entry. Consequently,

$$l(t) = \sqrt{Dt} \quad \text{with} \quad D = 2(P_{l=0} - P_L) \frac{c}{A} \quad (6)$$

The time  $t_0$  when the meniscus of the feeding channel reaches the junction is then given by  $l(t_0) = l_0$ , i.e.,

$$t_0 = \frac{l_0^2}{D} = \frac{A l_0^2}{2l P_L c} \quad (7)$$

where  $P_L$  is the Laplace pressure for the meniscus in the feeding channel, given by eq 4 with  $w = w_f$ .

To proceed, we assume that the junction is immediately filled and that the two menisci in the narrow and wide channels are formed instantaneously once the liquid reaches the junction. The Laplace pressure in the narrow channel,  $P_{L,n}$ , is less than the Laplace pressure in the wide channel,  $P_{L,w}$

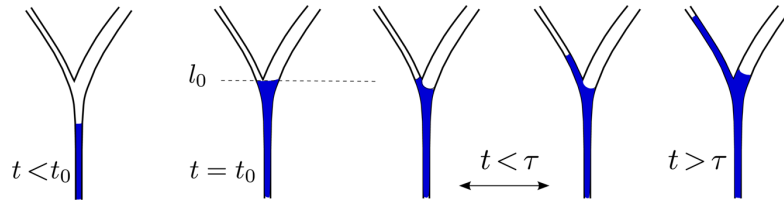


Figure 3. Different stages of menisci propagation along the time line.

$$P_{L,n} = -2\sigma \cos \theta \left( \frac{1}{w_n} + \frac{1}{\delta} \right) < -2\sigma \cos \theta \left( \frac{1}{w_w} + \frac{1}{\delta} \right) = P_{L,w} \quad (8)$$

Thus, the meniscus in the wide channel cannot propagate as long as the pressure in the junction,  $P_0$ , is less than  $P_{L,w}$ . Upon liquid invading the narrow channel, the pressure in the junction  $P_0$  rises from the initial value when the liquid arrives at the junction,  $P_0 = P_{L,n}$ . When the pressure in the junction reaches the pressure in the wide channel, the liquid also starts invading the wide channel. During this arrest time, the liquid in the narrow channel continues to rise until the distance  $l_{\text{resume}}$  measured from the junction is reached. It is expected that during spontaneous imbibition of asymmetric Y or T junctions the channel with the thinner width is filled first because it has the lower Laplace pressure. The displacement sequence in junctions with four channels could actually be different, as reported in ref 29, where the channel which is reached first by the contact line is filled first. In the Y-junction geometries that we consider, the latter is always the narrow channel.

The distance  $l_{\text{resume}}$  can be estimated using  $P_0 = P_{L,w}$ . Suppose the feeding channel and the junction are filled with liquid and the narrow channel is filled until a distance  $l_n$  from the junction. Then volume flux conservation at the junction requires  $Q = Q_f = Q_n$ , where  $Q_f$  and  $Q_n$  are the volume fluxes in the feeding and narrow channels, respectively:

$$Q_f = -\frac{P_0}{l_0} c_f = \frac{P_0 - P_{L,n}}{l_n} c_n = Q_n \quad (9)$$

$c_f$ ,  $c_n$ , and  $c_w$  are the constants in eqs 2 and 3 with  $w = w_f$ ,  $w_n$ , and  $w_w$ , respectively. This yields

$$P_0 = \frac{P_{L,n}}{1 + \frac{l_n c_f}{l_0 c_n}} \quad (10)$$

The condition  $P_0 = P_{L,w}$  for the meniscus in the wide channel to resume propagation is fulfilled when

$$\frac{l_{\text{resume}}}{l_0} = \frac{c_n}{c_f} \left( \frac{P_{L,n}}{P_{L,w}} - 1 \right) \quad (11)$$

Thus, the distance  $l_{\text{resume}}$  that the meniscus in the narrow channel has reached when the meniscus in the wide channel starts to propagate is proportional to the length of the feeding channel  $l_0$ .

The time that the meniscus in the narrow channel needs to propagate from the junction to the distance  $l_{\text{resume}}$  is the arrest time  $\tau$  of the meniscus in the wide channel. Inserting  $P_0$  from eq 10 into eq 5 yields

$$A \frac{dl_n}{dt} = \frac{|P_{L,n}|}{\frac{l_0}{c_f} + \frac{l_n(t)}{c_n}} \quad (12)$$

This equation describes the propagation of the meniscus in the narrow channel. After integration from  $t = t_0$ , when the meniscus first arrives at the junction, up to the time  $t = t_0 + \tau$ , when the meniscus at the narrow channel reaches the distance  $l_{\text{resume}}$ , we obtain the arrest time:

$$\tau = \frac{A}{|P_{L,n}|} \left\{ \frac{l_0 l_{\text{resume}} - l_0^2}{c_f} + \frac{l_{\text{resume}}^2 - l_0^2}{2c_n} \right\} = K l_0^2 \quad (13)$$

This equation is the equivalent of the scaling relation in a network of elongated pores<sup>19</sup> with  $l_{\text{resume}}$  from eq 11. Note that the arrest time is proportional to  $l_0^2$ , the square of the feeding length channel with a proportionality constant

$$K = \frac{A}{|P_{L,n}|} \left\{ \frac{c_n}{c_f} \left( \frac{P_{L,n}}{P_{L,w}} - 1 \right) + \frac{1}{2} \left( \frac{P_{L,n}}{P_{L,w}} - 1 \right)^2 - \frac{c_f}{c_n} - \frac{c_f^2}{2c_n^2} \right\} \quad (14)$$

Finally, when the meniscus in the wide channel resumes propagation at times  $t > t_0 + \tau$  the evolution of distances  $l_n(t)$  and  $l_w(t)$  of the meniscus in the narrow and wide channels, respectively, is determined by pressure  $P_0$  in the junction, which is determined by the mass balance condition for the flow

$$Q = Q_f = Q_n + Q_w \quad (15)$$

with  $Q_f = -P_0 c_f / l_0$ ,  $Q_n = (P_0 - P_{L,n}) c_n / l_n$ , and  $Q_w = (P_0 - P_{L,w}) c_w / l_w$ . One obtains

$$P_0 = \frac{\frac{P_{L,n} c_n}{l_n} + \frac{P_{L,w} c_w}{l_w}}{\frac{c_f}{l_0} + \frac{c_n}{l_n} + \frac{c_w}{l_w}} \quad (16)$$

and the equations of motion

$$A_j \frac{dl_j}{dt} = [P_0(l_n(t), l_w(t)) - P_{L,j}] \frac{c_j}{l_j(t)} \quad (17)$$

for  $j = n, w$ . Asymptotically one recovers the Lucas–Washburn behavior for both channels: For  $t \rightarrow \infty$ , one has  $l_j(t) \rightarrow \infty$  ( $j = n, w$ ) and thus  $P_0 \rightarrow 0$ . Consequently, 17 simplifies for large times to

$$A_j \frac{dl_j}{dt} = -P_{L,j} \frac{c_j}{l_j(t)} \quad \text{for } j = n, w \quad (18)$$

and therefore

$$l_n(t) = \sqrt{l_0^2 + D_n(t - t_0)} \\ l_w(t) = \sqrt{l_0^2 + D_w(t - (t_0 + \tau))} \quad (19)$$

with  $D_j = 2|P_{L,j}|c_j/A_j$  for  $j = n, w$ . The velocity of the moving menisci is obtained via

$$v_j(t) = \frac{D_j}{2\sqrt{D_j(t - (t_0 + \tau))}} \quad \text{for } j = n, w \quad (20)$$

The different stages of menisci propagation are shown in Figure 3.

#### 4. RESULTS AND DISCUSSION

In this section, we present our experimental results and compare them with our theoretical predictions. Figure 4 shows close-ups of the time series of a typical experiment. The liquid spontaneously invades the feeding channel; upon reaching the junction, the liquid fills the Y junction and the meniscus is split into two. Subsequently, the liquid invades first the narrow branch channel and after a certain arrest time  $\tau$  also invades the

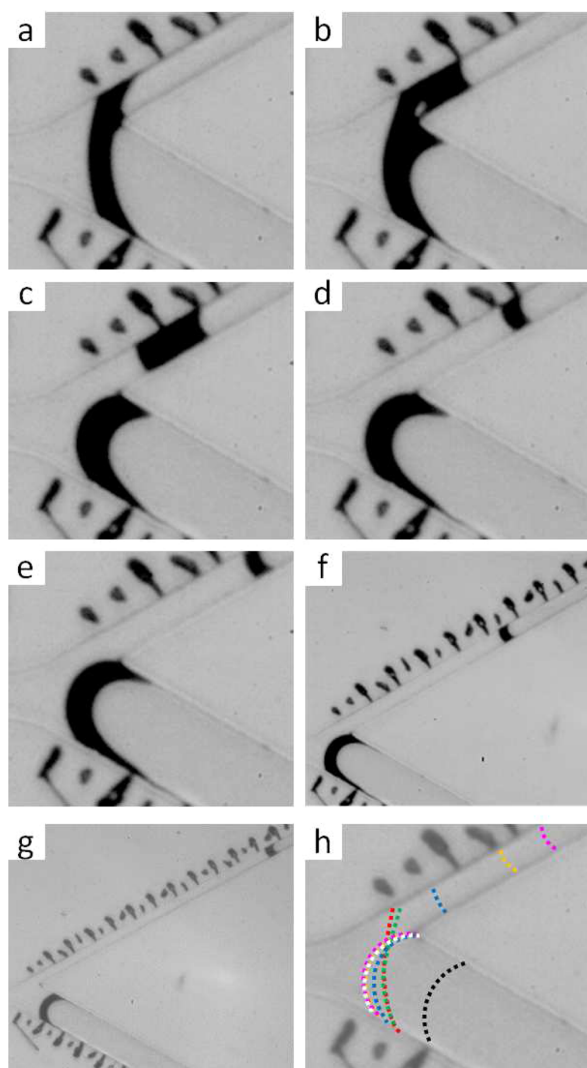


**Figure 4.** (a)–(g) Time series of FC-70 invading microfluidic Y-junction B1 in Table 1. Time steps are 0.02 s between images (a) and (e), whereas the time steps between images (e) and (f) and between (f) and (g) are 0.12 and 0.44 s, respectively. (h) Schematic representation of the meniscus evolution as extracted from the back side of the meniscus in tiles (a) red, (b) green, (c) blue, (d) yellow, (e) pink, (f) white, (g) black. Note that the meniscus is broad due to the slanted interface being a result of the out-of-plane curvature of the meniscus. The different ticks on the side of the branch channels are scaling marks with a pitch of about 50  $\mu\text{m}$ .

wide branch channel. During the arrest time, the length of the liquid in the narrow channel spreads upward a distance  $l_{\text{resume}}$  before the meniscus in the wide channel moves forward.

The Lucas–Washburn law does not satisfactorily describe the imbibition for very short liquid filament lengths, i.e., very short times.<sup>30–32</sup> The crossover time  $\tau^* = \rho r^2 / 4\eta^3$  from the Bosanquet regime to the Washburn regime is on the order of  $10^{-4}$  s for our experimental parameters and therefore negligible compared to the considered time scales for filling the feeding channel and the arrest times  $\tau$ . Also the Ohnesorge number  $Oh = \eta / (\rho r \sigma)^{1/2}$ , which reflects the ratio of viscous forces compared to capillary and inertia forces, is on the order of 10, suggesting that inertia forces are negligible. Thus, the experimentally analyzed lengths of the imbibing liquid filaments are sufficient long and it is justified to apply the Lucas–Washburn law for the theoretical description of the considered imbibition behavior.

A closer look at the meniscus evolution, as displayed in Figure 4h, reveals complex dynamics of the meniscus shape before and after it splits into two menisci, involving even intermittent backward motion of parts of the wide meniscus during the propagation of the small meniscus, as demonstrated more clearly in the time series depicted in Figure 5. Qualitatively, this behavior is similar to the dynamical evolution of the meniscus shape based on a diffuse interface model for capillary rise in a two-dimensional asymmetric junction.<sup>33</sup> The backward motion is more pronounced the larger the difference between  $w_w$  and  $w_n$  and the larger the feeding channel  $l_0$  and also leads to an experimental limitation of the length of the feeding channel as the large meniscus can even be dragged into the narrow channel. In our system this happens for channel length  $l_0$  larger than approximately 10 and 5.5 mm for branch channel ratios of  $w_w/w_n = 2.9$  and 1.8, respectively. For larger feeding channels the particular behavior of the liquid menisci in the junction is no longer negligible.

**4.1. Arrest Time and  $l_{\text{resume}}$ .** Experimentally, we identify the arrest time  $\tau$  as the difference between the time when two separate menisci first appear in the branched channels and the time when the meniscus in the wide channel starts moving forward.  $l_{\text{resume}}$  is then given by the distance the meniscus in the narrow channel advances in this time period. Our results for different feeding channel lengths ( $l_0$ ) and for different aspect ratios of the channel cross sections ( $w_w/w_n$ ) are shown in Figure 6(a).

The theoretical prediction for  $l_{\text{resume}}$ , according to eqs 11, 4, and 2, depends on  $l_0$ ,  $w_n$ ,  $w_w$ ,  $\epsilon_n$ , and  $\epsilon_f$  as

$$l_{\text{resume}} = l_0 \left( \frac{\delta + w_n w_w}{\delta + w_w w_n} - 1 \right) \frac{w_n^3 f(\epsilon_n)}{w_f^3 f(\epsilon_f)} \quad (21)$$

It turns out that the last factor  $f(\epsilon_n)/f(\epsilon_f)$  is very close to 1 for all parameters we used ( $1.03 < f(\epsilon_n)/f(\epsilon_f) < 1.09$ ), which is why we plotted in Figure 6(a)  $l_{\text{resume}}$  as a function of scaled variable  $l_0((\delta + w_n)/(\delta + w_w)(w_w/w_n) - 1)(w_n^3/w_f^3)$  for the experimental data listed in Table 1. According to eq 21,  $l_{\text{resume}}$  increases linearly with the length of the feeding channel  $l_0$ , which agrees nicely with experimental observations as demonstrated for  $l_{\text{resume}}$  varying by more than 1 order of magnitude.

According to the prediction of eq 13, the arrest time  $\tau$  should increase linearly with  $l_0^2$  for a fixed branch aspect ratio  $w_w/w_n$ . In Figure 4b the arrest time  $\tau$  is plotted as a function of  $l_0^2$  for two junction geometries with a fixed ratio of the branch

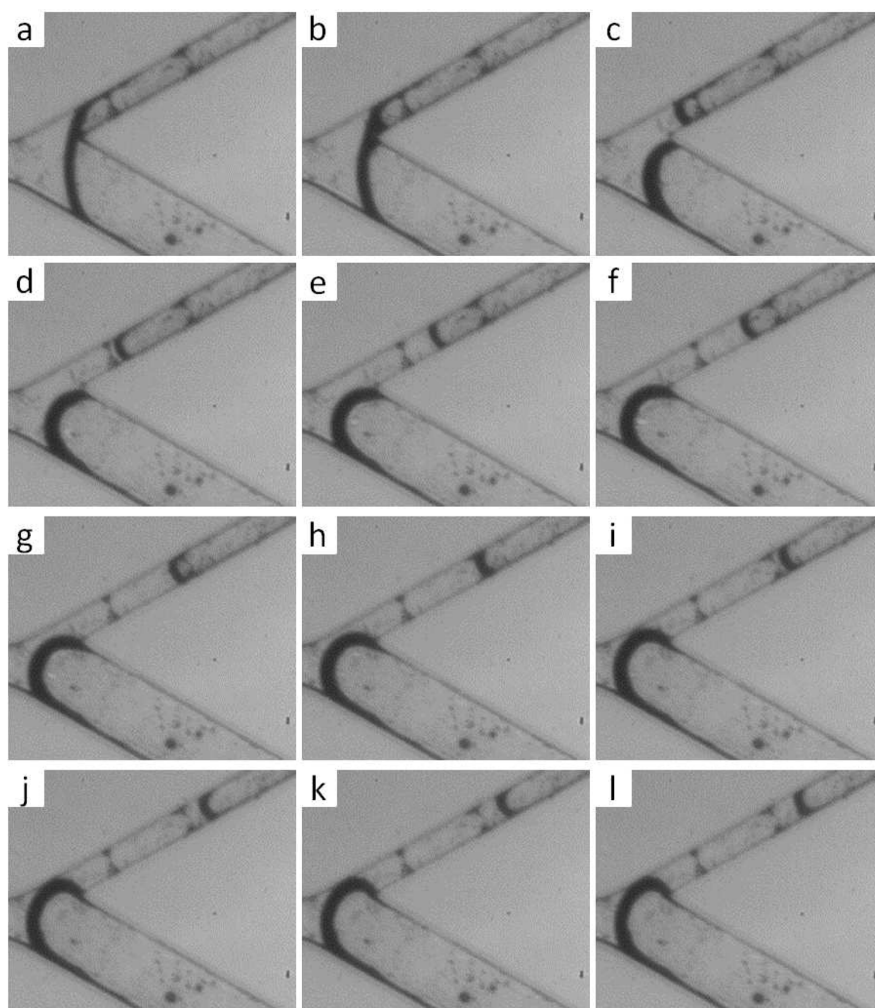


**Figure 5.** (a)–(l) Time series of FC-70 invading a microfluidic Y junction with a long feeding channel demonstrating the slow backward motion of the meniscus in the wide channel during the initial propagation of the meniscus in the narrow channel. The device used here is B4 (see table).

channels of  $w_w/w_n = 2.9$  and  $1.8$ , respectively, where the feeding channel length  $l_0$  was varied systematically up to the maximum length. The maximum length of the feeding channel  $l_0$  which can be analyzed for these junction geometries is limited by approximately  $5.5$  and  $10$  mm for branch channel ratios  $w_w/w_n$  of  $1.8$  and  $2.9$ , respectively. For larger feeding channels the meniscus of the wider channel is dragged into the narrow channel and the theoretical model loses its validity. The arrest times derived from all other channel geometries are in very good agreement with this scaling behavior but were varied only in a smaller range of feeding channel length  $l_0$ . Equation 13 is plotted as solid lines for the two Y-junction geometries, and we again achieve very good agreement between theoretical predictions and experimental data.

**4.2. Dynamical Evolution.** An example of the complete time evolution of menisci positions in the main feeding channel as well as in the wide and narrow channels of Y junctions with  $w_w/w_n \approx 3$  is presented in Figure 7 together with theoretical predictions. The large ratio of the channel width allows us to nicely discuss the characteristic behavior.

The liquid enters the feeding channel at  $x = 0$  and  $t = 0$ , and the time  $t_0$  at which the meniscus reaches the junction at  $x = l_0$  is indicated in Figure 7(a). The meniscus in the feeding channel is analyzed until it is clearly split into two menisci at the narrow and wide branches whereas the menisci in the two-branch channels are already analyzed when they touch the wall of the channels. Because of this analysis we obtain a small overlap of the three data sets which corresponds roughly to the extension of the junction. In our model, however, the volume of the junction is neglected. Thus, after the junction the theoretical data lag behind the experimental data as expected. To account for this time lag we subtract this difference from the experimental data. Moreover, an additional time shift of about  $0.1$ s for all setups takes into account the time the menisci need to adapt their shape to the channel geometry and orientation.

A fit of the Lucas–Washburn behavior, eqs 2–4 and 6, to the liquid meniscus imbining the feeding channel was used to determine the effective viscosity  $\eta_{\text{eff}}$  for each experiment. By this protocol we could absorb uncertainties in device or system parameters as discussed in the methods section and also

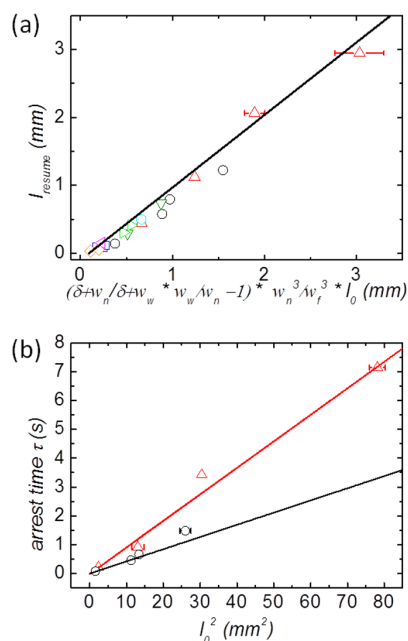


**Figure 6.** (a)  $l_{\text{resume}}$  as a function of the rescaled length of the feeding channel  $l_0$ , cf. eq 21. Experimental data are presented for junction geometries shown in Table 1. The line displays the theoretical prediction (group D ( $\square$ ), group A ( $\circ$ ), group B ( $\Delta$ ), group G ( $\nabla$ ), group C ( $\diamond$ ), E (left-pointing triangle), group F (right-pointing triangle), group H (hexagon)). (b) Arrest time  $\tau$  plotted as a function of  $l_0^2$  for two junction geometries A and B(B1–B4). (See Table 1.) The line displays the theoretical predictions according to eqs 13 and 14. Error bars in the  $x$  and  $y$  directions are omitted if they are smaller than the symbol size.

account for the differences in viscosity due to temperature variations. The thus-determined effective viscosity is used to derive the meniscus position in the narrow and wide channels using eqs 17. The agreement of the theoretical predictions and the experimentally obtained behavior is good throughout the entire imbibition of the Y junction.

In Figure 7 it can be seen that the meniscus in the wide channel remains arrested for time  $\tau$  until the other meniscus travels the distance  $l_{\text{resume}}$  in the narrow channel. The arrest time  $\tau$  and the corresponding  $l_{\text{resume}}$  are both indicated in Figure 7(a). From eq 13 one obtains an arrest time of  $\tau \approx 0.20$  s for the given example, which is in agreement with the corresponding experimental value of  $\tau = 0.22 \pm 0.02$  s. Figure 7(b) shows the filament length in the wide channel for three different feeding channel lengths  $l_0$ . The theoretically predicted and experimentally determined arrest time  $\tau$  are indicated by  $\tau_{\text{th}}$  and  $\tau_{\text{ex}}$  respectively. Both arrest times agree within the error bars, confirming the scaling relation  $\tau \approx l_0^2$  of ref 19. The error bar of the theoretical prediction  $\tau_{\text{th}}$  emerges from the uncertainties in  $l_0$ ,  $w_b$ ,  $w_w$ ,  $w_n$ ,  $w_w$ , surface tension  $\sigma$ , and effective viscosity.

Figure 8 shows the experimental velocity data for the two menisci in the narrow and wide channels and the theoretical prediction from eq 17 for a single experiment. As long as the meniscus in the wide channel remains arrested, the velocity is equal to zero in the theoretical prediction and only the velocity in the narrow channel can be provided. However, for times larger than  $\tau$ , the meniscus velocities in both the narrow and

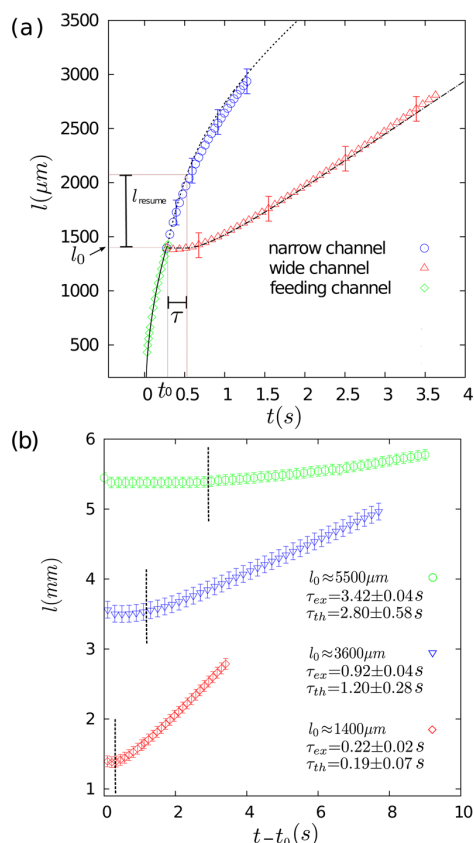


**Figure 7.** (a) Time evolution of the menisci positions in wide and narrow channels and the main feeding channels in device B1 (See Table 1.) The determined value for the effective viscosity is  $\eta_{\text{eff}} = 42.23$  mPa s. The solid, dotted, and dashed-dotted lines are the theoretical prediction via eq 19.  $\tau$  and  $l_{\text{resume}}$  are the corresponding theoretical predictions. Typical values of the error bars are shown for a few points. (b) Comparison between the arrest time  $\tau$  of similar devices with different feeding channel lengths  $l_0$  (group B). The amounts of  $l_0$  and the theoretical and experimental values of  $\tau$  are shown. Vertical lines show the corresponding arrest time  $\tau_{\text{th}}$ . The large error bars represent the uncertainty in the length of the feeding channel  $l_0$ ; this error is constant for all data points.

wide channels can be described. In fact, the agreement between the experimental results and theoretical prediction is very good up to the interval in which the meniscus in the wide channel is slightly moving backward (as is visible in Figure 5), which was neglected in the theory. Theoretically, the time when the velocity of the wide meniscus becomes larger than zero determines the arrest time  $\tau$ .

## 5. CONCLUSIONS

We studied spontaneous imbibition behavior in asymmetric microfluidic Y junctions. We found that the meniscus in the wide channel is arrested for a time that is proportional to the time the meniscus of the feeding channel needs to reach the junction (i.e., proportional to the square of the feeding length channel). The distance  $l_{\text{resume}}$  that the meniscus in the narrow channel propagates from the junction until the meniscus in the wide channel starts to move forward is found to be proportional to the feeding channel length. These experimental observations agree quantitatively with theoretical predictions

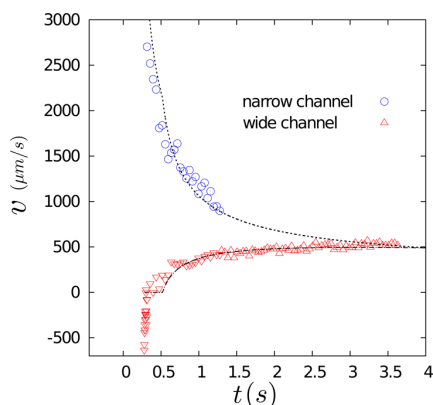


**Figure 8.** Velocity of menisci in wide and narrow channels in the same sample of Figure 7(a). The experimental data for the narrow branch channel end at  $t \approx 1.3$  s when the meniscus leaves the field of view. The dotted and dashed lines are the predictions of the model for narrow and wide channels, respectively.

based on a simple model involving Poiseuille flow in all three channels and neglecting the complex meniscus dynamics inside the junction, which is justified as long as the dimensions of the junctions are small as compared to the channel length. Using the viscosity as a fit parameter for the dynamical evolution in all three channels, the proportionality constants of experiment and theory also agree quantitatively.

It has been hypothesized that long-lasting meniscus arrests are possibly the physical origin of anomalously fast imbibition front broadening in nanoporous Vycor glass.<sup>18,19</sup> Here we have provided the first experimental evidence that the basic ingredients of the scaling theory for imbibition front broadening in pore networks with elongated pores<sup>19</sup> is indeed correct, as the experimental data of Figure 6 confirm the scaling relation  $\tau \propto l_0^2$ .<sup>19</sup> Concomitantly, we also found that for extremely elongated pores new physics beyond meniscus arrest might occur, namely, when the backward motion of the meniscus in the wide junction is so strong that the entrainment of air/gas bubbles into the narrow meniscus occurs. A detailed study of the entrainment process in asymmetric junctions with long feeding channels as well as its implication for spontaneous imbibition in pore networks remains for a forthcoming study.

## AUTHOR INFORMATION

### Corresponding Author

\*E-mail: [sadjadi@lusi.uni-sb.de](mailto:sadjadi@lusi.uni-sb.de)

### Notes

The authors declare no competing financial interest.

## ACKNOWLEDGMENTS

This work is supported by German Research Foundation DFG via grant no. GRK1276.

## REFERENCES

- Alava, M.; Dubé, M.; Rost, M. Imbibition in disordered media. *Adv. Phys.* **2004**, *53*, 83.
- Sahimi, M. *Flow and Transport in Porous Media and Fractured Rock*; Wiley-VCH: Weinheim, 2011.
- Bear, J. *Dynamics of Fluids in Porous Media*; Elsevier: New York, 1972.
- Todd, D. K.; Mays, L. W. *Groundwater Hydrology*; John Wiley, 2005.
- Lucas, R. Über das Zeitgesetz des kapillaren Aufstiegs von Flüssigkeiten. *Kolloid-Z.* **1918**, *23*, 15.
- Washburn, E. W. The dynamics of capillary flow. *Phys. Rev.* **1921**, *17*, 273.
- Dimitrov, D. I.; Milchev, A.; Binder, K. Capillary Rise in Nanopores: Molecular dynamics evidence for the Lucas-Washburn equation. *Phys. Rev. Lett.* **2007**, *99*, 054501.
- Gruener, S.; Hofmann, T.; Wallacher, D.; Kityk, A. V.; Huber, P. Capillary rise of water in hydrophilic nanopores. *Phys. Rev. E* **2009**, *79*, 067301.
- Reyssat, M.; Courbin, L.; Reyssat, E.; Stone, H. A. Imbibition in geometries with axial variations. *J. Fluid. Mech.* **2008**, *615*, 335.
- Dullien, F. A. L. *Porous Media, Fluid Transport and Pore Structure*; Academic Press: San Diego, 1992.
- Dubé, M.; Rost, M.; Alava, M. Conserved dynamics and interface roughening in spontaneous imbibition: Critical overview. *Eur. Phys. J. B* **2000**, *15*, 691.
- Geromichalos, D.; Mugele, F.; Herminghaus, S. Nonlocal dynamics of spontaneous imbibition fronts. *Phys. Rev. Lett.* **2002**, *89*, 104503.
- Buldyrev, S. V.; Barabási, A. L.; Caserta, F.; Havlin, S.; Stanley, H. E.; Vicsek, T. Anomalous interface roughening in porous media: Experiment and model. *Phys. Rev. A* **1992**, *45*, R8313.
- Horvath, V. K.; Stanley, H. E. Temporal scaling of interfaces propagating in porous media. *Phys. Rev. E* **1995**, *52*, S166.
- Hernandez-Machado, A.; Soriano, J.; Lacasta, A. M.; Rodrez, M. A.; Ramz-Piscina, L.; Ort, J. Interface roughening in Hele-Shaw flows with quenched disorder: Experimental and theoretical results. *Europhys. Lett.* **2001**, *55*, 194.
- Gelb, L. D.; Gubbins, K. E. Characterization of porous glasses: Simulation models, adsorption isotherms, and the Brunauer-Emmett-Teller analysis method. *Langmuir* **1998**, *14*, 2097.
- Song, Y. Q.; Ryu, S.; Sen, P. N. Determining multiple length scales in rocks. *Nature* **2000**, *406*, 178.
- Gruener, S.; Sadjadi, Z.; Hermes, H. E.; Egelhaaf, S. U.; Knorr, K.; Kityk, A. V.; Rieger, H.; Huber, P. Anomalous front broadening during spontaneous imbibition in a matrix with elongated pores. *Proc. Nat. Acad. Sci. U.S.A.* **2012**, *109*, 10245.
- Sadjadi, Z.; Rieger, H. Scaling theory for spontaneous imbibition in random networks of elongated pores. *Phys. Rev. Lett.* **2013**, *110*, 144502.
- Armstrong, R. T.; Berg, S. Interfacial velocities and capillary pressure gradients during Haines jumps. *Phys. Rev. E* **2013**, *88*, 043010.
- Lenormand, R.; Zarcone, C.; Sarr, A. Mechanisms of the Displacement of one fluid by another in a network of capillary ducts. *J. Fluid Mech.* **1983**, *135*, 337.
- Chatzis, I.; Dullien, F. A. L. Dynamic immiscible displacement mechanisms in pore doublets: theory versus experiment. *J. Colloid Interface Sci.* **1983**, *91*, 199.
- Sorbie, K. S.; Wu, Y. Z.; McDougall, S. R. The Extended Washburn Equation and Its Application to the Oil/Water Pore Doublet Problem. *J. Colloid Interface Sci.* **1995**, *174*, 289.
- Xia, Y.; Whitesides, G. M. Soft Lithography. *Annu. Rev. Mater. Res.* **1998**, *28*, 153–184.
- Product information sheet from 3M.
- <http://imagej.nih.gov/ij/>.
- Brody, J. P.; Yager, P.; Goldstein, R. E.; Austin, R. H. Biotechnology at low Reynolds numbers. *Biophys. J.* **1996**, *71*, 3430–3441.
- White, F. M. *Viscous Fluid Flow*; McGraw-Hill: New York, 1974.
- Chapman, E. M.; Yang, J.; Crawshaw, J. P.; Boek, E. S. Pore Scale Models for Imbibition of CO<sub>2</sub> Analogue Fluids in Etched Micro-Model Junctions Using Micro-Fluidic Experiments and Direct Flow Calculations. *Conference Proceedings of the AIChE Annual Meeting*, 2013; Vol. 37, p 3680.
- Quere, D. Inertial capillarity. *Europhys. Lett.* **1997**, *39*, 533–538.
- Stange, M.; Dreyer, M. E.; Rath, H. J. Capillary driven flow in circular cylindrical tubes. *Phys. Fluids* **2003**, *15*, 2587–2601.

(32) Kornev, K. G.; Neimark, A. V. Spontaneous Penetration of Liquids into Capillaries and Porous Membranes Revisited. *J. Colloid Interface Sci.* **2001**, *235*, 101–113.

(33) Mehrabian, H.; Gao, P. P.; Feng, J. J. Wicking flow through microchannels. *Phys. Fluids* **2011**, *23*, 122108.